Poking Membrane, Necking Tether

Thomas R. Powers,[1,†] Greg Huber,[2,‡] and Raymond E. Goldstein[3,§]

[1] *Division of Engineering, Brown University, Providence, RI 02912*

[2] *Department of Physics, UMass Boston, Boston MA 02125*

[3] *Department of Physics and Program in Applied Mathematics, University of Arizona, Tucson, AZ 85721*

(Dated: September 9, 2001)

Thin cylindrical tethers are ubiquitous structures in lipid bilayer membranes, arising in situations ranging from micromanipulation experiments on artificial vesicles to the dynamic structure of the Golgi apparatus. We study the shape and formation of a tether in a simplified situation: an initially flat membrane disk under tension subject to a point force. We show how a tether forms from the elastic boundary layer near the point of application of the force for sufficiently large displacement.

PACS numbers: 87.16.Dg, 87.17.Aa, 02.40.-k

I. INTRODUCTION

Imagine a soap film connecting two nearby parallel rings which are slowly pulled apart. The film evolves through a series of catenoid shapes until the ring separation reaches a critical value; then the film breaks. Now imagine performing the same experiment with microscopic rings connected by a lipid bilayer membrane. In this paper we will show that the membrane forms catenoid shapes at small ring separations, but instead of breaking, the membrane forms a thin cylindrical tether for sufficiently large displacement.

A situation very much like this thought experiment arises in a host of real experiments on artificial vesicles, living cells, and membranous organelles such as the Golgi apparatus. Perhaps the most controlled tether experiment is that of Evans and Yeung, in which a tether forms when a micropipet is withdrawn from a spherical vesicle held at a fixed tension and bonded to a stationary bead [1]. There are many variants on this experiment [2–6], and such experiments have been used to measure a wide variety of membrane mechanical properties [7].

Tethers commonly form in less controlled situations as well. Simply pulling on a vesicle or cell with a sufficiently large point force leads to a membrane tether (Fig. 1). Tethers form when tubulin trapped inside a vesicle polymerizes to form microtubules [8]; as the microtubules grow, the initially spherical membrane at first distorts into an ellipsoidal shape, and then eventually forms a surface of revolution with a contour in the shape of the Greek letter "ϕ" [9–11]. Improvements in staining techniques have recently revealed dynamic tether networks in the Golgi apparatus of living cells [12]; similar model membrane networks have been studied *in vitro* [13] and used as templates for making more durable networks [14].

Despite much theoretical, computational, and experimental attention, a simple picture for tether formation has not yet emerged. The goal of this paper is to provide such a picture. The variety of conditions under which tethers occur shows that they are robust structures, insensitive to the details of applied forces and boundary conditions. It is therefore natural to study tethers theoretically in the simplest possible situation, namely the classic soap film geometry described above (Fig. 2). This model situation captures the essential features of the tether shape and formation without the experimentally important but ultimately complicating effects such as volume and lipid conservation. Our quasi-analytic approach exploits the smallness of the tether radius, and is complementary to important numerical work by various groups, most notably Heinrich *et al.* [6]. We begin our analysis in section II with a discussion of shells, balloons, and soap films in order to contrast their familiar mechanical properties with the peculiar properties of lipid bilayer membranes. The latter are the subject of section III, where we define precisely our model problem. Section IV reviews the elements of the soap film problem which are relevant for understanding the formation of tethers, which we consider in section V. There we use asymptotic methods to solve the linearized equations for small ring displacements and large tensions, and find that the membrane shape is that of a catenoid with a small elastic boundary layer surrounding the smaller ring (the point force). At a critical ring separation, a tether forms from the elastic boundary layer. We study the tether shape analytically and numerically and make contact with the classic matched asymptotics film coating calculations of Landau and Levich [15], as well as Bretherton's related calculation of the shape of a long air bubble rising in a fluid-filled capillary tube [16]. Section VI contains a discussion of our results and their relation to previous work. We conclude in section VII. The appendix reviews

[†] Electronic address: Thomas_Powers@brown.edu

[‡] Electronic address: huber@umb.edu

[§] Electronic address: gold@physics.arizona.edu

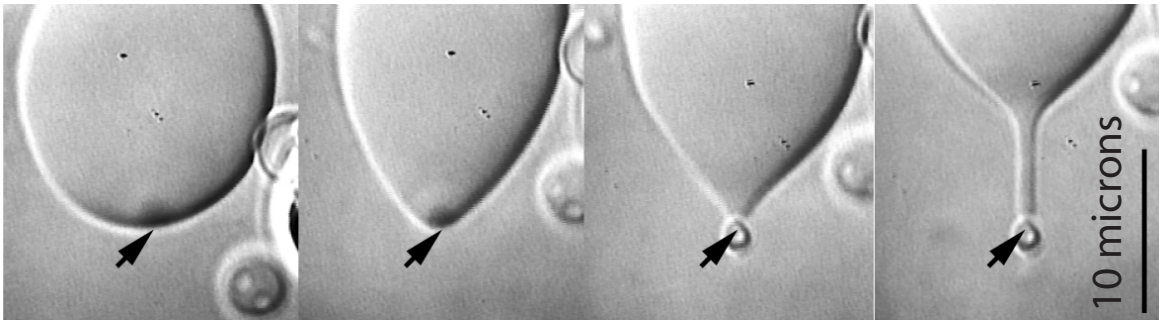

FIG. 1: Equilibrium shapes of a vesicle subject to various point forces. An optical tweezer exerts the point force, which increases from left to right. Figure courtesy of D. Fygenson.

the subtleties that arise when comparing the variational approach for lipid bilayer membrane elasticity to that of moment and force balance.

II. SHELLS, BALLOONS, AND SOAP FILMS

Before exploring the lipid bilayer membrane properties that give rise to tethers, we review three examples of elastic surfaces encountered at the macroscopic scale: shells, balloons, and soap films. Much of our intuition about elastic surfaces derives from these canonical examples. Some of this intuition can be directly applied to lipid membranes, but it is illuminating to point out the crucial differences as well.

Shells are solid surfaces with a small thickness and a preferred shape in the absence of external stresses. A plate is a shell with a flat preferred shape. It is a matter of common experience that the force required to bend a thin plate through a certain displacement is much less than that required to stretch the plate through the same displacement. The plate can undergo large displacements through bending without subjecting each element to large stress; thus, linear elasticity is valid and the nonlinearities in the equations for shape are solely geometrical. In the limit of small plate thickness, stretching energy exceeds bending energy, since bending is differential stretching. The lowest energy deformations are the so-called isometric deformations that have no stretching [17]. For example, the axisymmetric isometric deformations of the plane are cylinders and cones [18]. Note that a shearing motion locally stretches the plate, even if the total area does not change. Bending energy (and possibly boundary conditions) removes the degeneracy when, as in the case of a flat plate, there is a multiplicity of isometric deformations. Bending also plays a role near boundaries and point forces. A familiar example of a plate with vanishing thickness is a sheet of paper, which bends easily but hardly stretches or shears. The reader can easily verify that a sheet of paper subject to a point force forms a cone with a single fold, a shape with two-fold symmetry. (One way to balance the point force is to place the sheet on circular rim [19].) For shells, the isometric constraint on deformations is even more severe. *Any* deformation of a sphere requires some local stretching or shearing: no almost-spherical shapes are isometric to the sphere. A spherical shell is *geometrically rigid*. On the other hand, there are isometric small deformations of spherical shell with a circular hole [17]. The problem of determining the geometric rigidity of an axisymmetric shell with boundaries was solved using the qualitative theory of differential equations [20]; for recent progress using a geometric approach which can be generalized to non-axisymmetric shells, see [21].

Next, consider the case of balloons. Like plates with vanishing thickness, there is virtually no cost to bending a section of a balloon compared to that of stretching or shearing. However, deformations are not required to be isometric since the cost of stretching is also low. Such a material is called a "membrane" in the theory of elasticity [17]; to avoid confusion with lipid bilayer membranes we will not use this terminology. Since real balloons are easily stretched out of the linear elastic regime, the nonlinearity of the governing equations arises from the constitutive relations as well as the geometry of large deformations. Anyone who has inflated a cylindrical balloon has seen a phenomenon very much like the tethers of Fig. 1. A partially inflated balloon has two cylindrical regions, one smaller than the other, which are smoothly connected by a junction region. However, this phenomenon differs fundamentally from that of tether formation in lipid bilayer membranes for several reasons. No point force is required to make a balloon form atether; it arises from the nonlinear constitutive relation between tension and areal extension, which is reflected by a nonmonotonic p-V curve, reminiscent of the isotherms of the van der Waals equation of state for a gas [22]. The material in the larger cylinder is stretched more, and thus has a higher tension. The smaller cylinder is under smaller tension; the difference between the axial force of each

tension is precisely balanced by the net pressure on the junction region. Thus, a pressure jump across the surface of the balloon is crucial for this tether; we will see below that such a pressure jump is unnecessary for lipid bilayer membrane tethers.

Our final canonical example is the soap film. We will consider "ideal" soap films, which simply minimize area subject to the boundary conditions and volume constraints. We disregard effects such as thickness variations and draining, because these effects do not have a clear counterpart in the case of lipid bilayer membranes. Since soap films are liquid, the static in-plane shear rigidity vanishes, and the notion of geometric rigidity does not apply. Deformations need not be isometric and folds are not required to bend a flat film into a hemisphere. (There can be solid-like folding behavior in liquid film dynamics whenever bending flows are preferable to extensional flows [23].) Unlike the case of plates, interfacial tension is a material property of the soap film, and is not determined by external forces. To imagine poking a soap film with a point force, consider again the geometry of two rings described in the introduction, but now take one ring radius to be much smaller than the other. Equilibrium solutions exist only when the ring separation is less than a critical separation, comparable to the radius of the smaller ring. At a slightly larger separation, the film breaks. The equilibrium shapes are shallow catenoids, and look nothing like tethers (structures reminiscent of thin tethers form during the rupture of a soap film, but these have a dynamical origin; see [24]). However, these shallow catenoid shapes resemble the junction region between the tether and vesicle of Fig. 1. Soap films and catenoids will be studied more fully in section IV.

As we shall see next, lipid bilayer membranes have elements of each of these examples. Like macroscopic plates, lipid membranes resist bending, but they are typically fluid and therefore lack geometric rigidity, like soap films. The interplay between these solid-like and fluid properties leads to the formation of tethers.

III. LIPID BILAYER MEMBRANES

A Bending elasticity

There is a vast literature on the mechanics of lipid bilayer membranes (*e.g.* see [25]). We will only review the aspects relevant to tethers. Lipid molecules are amphiphilic, composed of two oily hydrophobic chains attached to a polar hydrophilic head. Lipids self-assemble in solution to shield the chains from the water, forming micron-size bilayer surfaces. In the fluid phase, a typical self-diffusion constant for a lipid molecule in a membrane is of order $10^{-8}\mathrm{cm}^2/\mathrm{sec}$ [26]. The membrane is clearly a two-dimensional fluid over the time scale of typical tether experiments: a molecule will diffuse from one side of a one micron radius spherical vesicle to the other in about a second. Hence, there is no in-plane static shear modulus. However, membranes have a non-zero bending modulus since bending the membrane compresses and extends the slightly elastic heads and tails of the lipid molecules. The fluid nature of the membrane constrains the form of the elastic energy to depend only on the *shape* of the membrane. To lowest order in curvatures, the bending energy is given by the expression of Canham and Helfrich [27, 28],

$$\mathcal{E}_{\mathrm{el}} = \int \mathrm{d}S \left[\frac{\kappa}{2}(2H)^2 + \frac{\bar{\kappa}}{2} K \right], \tag{1}$$

where H is the mean curvature of the membrane surface, and K is the Gaussian curvature. In terms of the principal radii of curvature R_1 and R_2 at a point on the surface, $2H = 1/R_1 + 1/R_2$ and $K = 1/(R_1 R_2)$. Explicit formulas for these curvatures will be given below. For simplicity, we suppose that there is no difference between the two sides of the bilayer; hence, there is no spontaneous curvature. The Gaussian curvature term is typically dropped in studies of vesicles since it amounts to the sum of a deformation-independent term and a boundary term by the Gauss-Bonnet theorem:

$$\int \mathrm{d}S K = 4\pi(2-2g) + \oint \mathrm{d}s \kappa_g, \tag{2}$$

where the genus g is the number of handles and κ_g is the geodesic curvature of the boundary of the surface [18]. Note that a more detailed treatment of the formation of tethers in vesicles would require additional terms of the generalized bilayer couple model [29–33]. In the spirit of explaining tether formation in the simplest possible context, we disregard these.

Although typical values for the elastic bending modulus κ are 10–15k_BT, thermal fluctuations easily excite

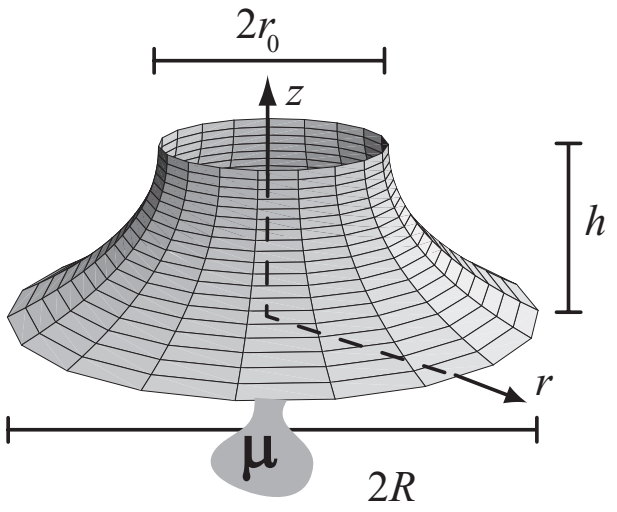

FIG. 2: Model problem. Two parallel rings with aligned centers are connected by a lipid bilayer membrane in contact with a lipid reservoir at fixed chemical potential μ.

long wavelength bending modes since the elastic energy vanishes as the fourth power of the wavenumber for fluctuations about a flat sheet. These fluctuations lead to an entropic area elasticity similar to that of semiflexible polymers, as is most directly illustrated by the experiments of Evans and Rawicz [34] (see also [35]). In these experiments, the tension in a vesicle is measured as a function of apparent area by suctioning a small amount of the vesicle membrane into a pipet. At low suctions (or low tensions), the resistance to stretching is the entropic penalty of reducing the number of fluctuating modes. At high tensions, most of the thermal ripples have been pulled out of the membrane, and the resistance to stretching is mainly due to the membrane's intrinsic area elasticity. We consider here the high tension regime only, and therefore disregard thermal fluctuations.

B Model problem and nondimensionalization

As in the introduction, we consider a lipid membrane spanning two rings that are initially concentric and lying in the plane $z = 0$ (see Fig. 2). The outer ring of radius R remains in this plane, but the height h_0 of the inner ring will be varied. Measuring all lengths in units of the radius R we henceforth set $R = 1$. The inner ring then has radius $r_0 \ll 1$. Later, we will take $r_0 \to 0$ to recover the result of a point force, but for comparison with the case of soap films and also for our numerical approach it is convenient to keep r_0 nonzero for now. We assume that there is a reservoir of lipid at a fixed chemical potential μ, and further suppose this "tension" is very large compared to the bending elasticity, $\mu \gg \kappa$ (justifying our neglect of thermal fluctuations). Since the membrane has edges, the Gaussian modulus $\bar{\kappa}$ affects the shape through the boundary conditions (recall the geodesic curvature term of Eq. (2)). For simplicity, we disregard this effect and set $\bar{\kappa} = 0$.

Our model is closest in spirit to the tether experiments of Evans and Yeung [1] mentioned earlier. The pipet suction sets the value of the tension μ, and the small amount of lipid projecting inside the pipet serves as a reservoir. In the experiments the vesicle is under pressure and is therefore curved, whereas in our model there is no pressure jump across the initially flat membrane. The role of the pressure in vesicle tethers is small since the tether curvature is much larger than the vesicle curvature for high tension; in fact, below we show that the pressure jump leads to a subleading correction to the tether radius.

To complete the specification of the model problem, we must define the boundary conditions at the rings. The tangent plane of the surface at the point force is perpendicular to the force if the line of action is along the axis of symmetry. Since the role of the small ring is to mimic a point force, the membrane is clamped so that the tangent plane at each point on the boundary with the small ring is in the plane of the small ring. The ring at $r = 1$ is somewhat artificial; therefore we choose the simplest possible boundary condition for $r = 1$, which turns out to be zero moment, $H = 0$ [17]. The outer ring acts as a hinge. Defining

$$\epsilon \equiv \frac{\kappa}{\mu}\,, \tag{3}$$

our task is to minimize

$$\mathcal{E} = \int \mathrm{d}S + \frac{\epsilon}{2}\int \mathrm{d}S(2H)^2 \tag{4}$$

for given ring separation h_0 subject to the boundary conditions and $\epsilon \ll 1$. Equation (4) casts the tether problem into the same form as the classic calculus of variations problem for a minimal surface ($\epsilon = 0$).

C Euler-Lagrange equations

The derivation of the Euler-Lagrange equations from the energy of Eq. (4) is somewhat lengthy but straightforward [36],

$$2\epsilon(\nabla^2 H + 2H^3 - 2HK) - 2H + \Delta p = 0, \tag{5}$$

where ∇^2 is the covariant Laplacian on the surface. Δp (measured in units of $\mu/R = \mu$) is zero for our soap film geometry, but it is included in Eq. (5) for later discussion of the effect of pressure on tether shape. Note that $\epsilon = 0$ and $\Delta p = 0$ yields the minimal surface equation, $H = 0$. Since the membrane shape is a surface of revolution, natural coordinates for the surface are φ, the azimuthal angle, and s, arc-length along a meridian. Arclength is measured from the inner ring, which has coordinate $s = 0$. The position of a point on the surface is therefore $\mathbf{X}(s,\varphi) = r(s)\hat{\mathbf{r}} + z(s)\hat{\mathbf{z}}$, where r and z are cylindrical coordinates. Note that $r_s^2 + z_s^2 = 1$, since s is arclength.

With these choices, the metric or first fundamental form is

$$g_{ij}\mathrm{d}\xi^i\mathrm{d}\xi^j = \mathrm{d}s^2 + r^2\mathrm{d}\varphi^2, \tag{6}$$

where $\xi^1 = s$ and $\xi^2 = \varphi$. The second fundamental form is

$$K_{ij}\mathrm{d}\xi^i\mathrm{d}\xi^j = (z_s r_{ss} - r_s z_{ss})\ \mathrm{d}s^2 - r z_s \mathrm{d}\varphi^2, \tag{7}$$

where $z_s = \mathrm{d}z/\mathrm{d}s$, *etc.* We follow the usual conventions for raising and lowering indices using the inverse g^{ij} of the metric tensor. Thus, $g^{ik}g_{kj} = \delta^i_j$, $K^i_j = g^{ik}K_{kj}$, and

$$H \equiv \frac{1}{2}g^{ij}K_{ij} = \frac{1}{2}\left[\frac{r_{ss}}{z_s} - \frac{z_s}{r}\right], \tag{8}$$

$$K \equiv \det K^i_j = -\frac{r_{ss}}{r}, \tag{9}$$

$$\nabla^2 \equiv \frac{1}{\sqrt{g}}\partial_i g^{ij}\sqrt{g}\partial_j = \frac{1}{r}\frac{\mathrm{d}}{\mathrm{d}s}r\frac{\mathrm{d}}{\mathrm{d}s}, \tag{10}$$

where g is the determinant of the metric tensor g_{ij}, and $r_s^2 + z_s^2 = 1$ was used to simplify (8).

The Euler-Lagrange equation (5) for an axisymmetric shape is a nonlinear ordinary differential equation, easily solved with numerical methods. However, we can gain more insight by exploiting the smallness of ϵ. Since it multiplies the term in (5) with the highest number of derivatives, we expect a boundary layer wherever the boundary conditions are incompatible with Eq. (5) with $\epsilon = 0$. It is now clear why the zero moment $H = 0$ boundary condition *is* the most natural condition at the larger ring; this boundary condition is compatible with the minimal surface equation and does not lead to a boundary layer at the larger ring. The clamped boundary condition at the smaller ring, however, is incompatible with the minimal surface equation, since the ring must exert a moment on the surface to keep it clamped. In this inner region, bending and tension balance and the shape is determined by the full Euler-Lagrange equation, where the smallness of ϵ is offset either by rapid variations as a function of s or the smallness of the tether radius. In the outer region, beyond the elastic boundary layer, bending is unimportant and the shape is governed by the minimal surface equation, $H = 0$. The only nonplanar axisymmetric minimal surface is a catenoid, the surface of revolution generated by a catenary curve [18]. Thus, the membrane forms a catenoid in the outer region. In the next section we review basic facts about catenoids.

IV. CATENOID LORE

We noted in the previous section that setting $\epsilon = 0$ and $\Delta p = 0$ in Eq. (5) results in the minimal surface equation $H = 0$. To leading order, the outer solution to Eq. (5) is given by the exactly the same condition. The solution to the minimal surface equation is conveniently found by applying Noether's theorem directly to the energy functional (4) with $\epsilon = 0$. To this end, we rewrite $\mathrm{d}S$ in terms of $r(z)$:

$$\mathcal{E} = \int \mathrm{d}\varphi \mathrm{d}z r\sqrt{1 + r_z^2}. \tag{11}$$

The conserved quantity associated with the invariance of the integrand of (11) with respect to translations in z is the axial force F:

$$\frac{F}{2\pi} = \frac{r}{\sqrt{1 + r_z^2}}. \tag{12}$$

The radius r attains its minimum value $b = F/(2\pi)$ when $r_z = 0$. Integrating (12) yields the catenoid

$$r = b\cosh\left(\frac{z - c}{b}\right), \tag{13}$$

where c is the z-coordinate of the minimum radius. Note that b is the minimum *possible* radius; *i.e.* it is possibly

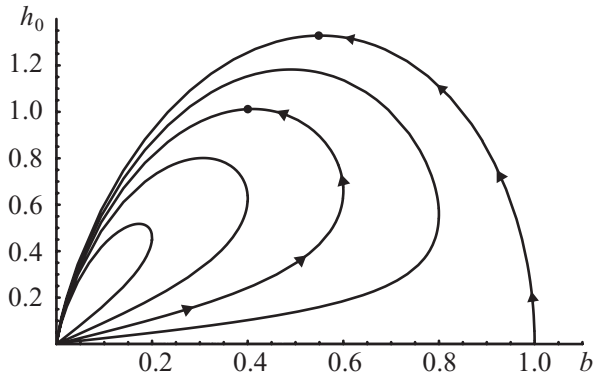

FIG. 3: Ring separation h_0 *vs.* minimum neck radius b (force over 2π) for the values $r_0 = 0.2, 0.4, 0.6, 0.8$, and 1.0 proceeding from the innermost curve to the outermost curve. For a given r_0, as the rings are separated, the sequence of shapes corresponds to the trajectory marked with arrows.

not attained. The minimum radius is attained only if $c \le h_0$.

The boundary condition $r(0) = 1$ determines $c = \pm\cosh^{-1}(1/b)$, and thus Eq. (13) expands to

$$r = \cosh\left(\frac{z}{b}\right) \mp \sqrt{1 - b^2}\sinh\left(\frac{z}{b}\right). \tag{14}$$

We choose the upper sign since it corresponds to catenaries with a minimum neck radius at a positive value of z ($c > 0$). The force F, or equivalently the minimum neck radius b, is determined by the boundary condition at the other ring: $r(h_0) = r_0$, or

$$r_0 = \cosh\left(\frac{h_0}{b}\right) - \sqrt{1 - b^2}\sinh\left(\frac{h_0}{b}\right). \tag{15}$$

Solving (15) for h_0 gives the separation as a function of force:

$$h_0 = b\log\left(\frac{r_0 \pm \sqrt{r_0^2 - b^2}}{1 - \sqrt{1 - b^2}}\right). \tag{16}$$

Note that the two branches form a closed curve in the b-h_0 plane for $r_0 < 1$ (Fig. 3). Since each curve has a maximum (marked with a dot for the curves $r_0 = 0.6$ and $r_0 = 1.0$), there is a critical r_0-dependent separation beyond which no catenoid solution exists. The soap film spanning the two rings breaks just beyond this critical separation. For fixed r_0 and a given separation h_0 below the maximum, there are two catenoid solutions. For example, Fig. 4 illustrates the two equilibrium catenoid shapes with $r_0 = 1$ and $h_0 = 0.6$. For a given h_0, one can show that the catenoid with the larger b has less area. Thus, the solution with the smaller neck (*e.g.* the upper catenoid in Fig. 4) is unobservable in real soap films. In the presence of bending stiffness and a fully developed

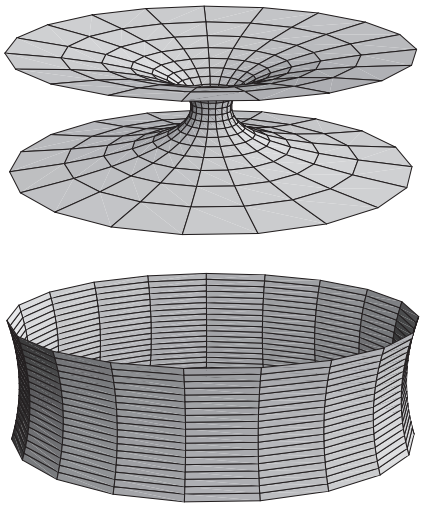

FIG. 4: The two catenoid solutions with equal size rings ($r_0 = 1$) and ring spacing $h_0 = 0.6$; the lower catenoid has less area.

tether, we shall see below that the axial force is $2\pi\sqrt{2\epsilon}$. To see which catenoid matches onto a fully developed tether, consider the extreme case $r_0 = 1$. Since the axial force vanishes as $\epsilon \to 0$, the matching catenoid must have b near zero and lie on the left branch of the $r_0 = 1$ curve of Fig. 3. By continuity, as r_0 decreases, the corresponding matching catenoid is always on the left branch. Therefore, the catenoid joining a tether is the one with a narrow neck; bending stiffness selects this otherwise unobservable shape.

Finally, the arrows in Fig. 3 display the trajectory of shapes as the rings are separated. The force F increases from zero to a maximum value, and then decreases slightly before the film breaks. We shall see that this nonmonotonic behavior occurs in the case of tethers as well.

V. FROM CATENOIDS TO TETHERS

As discussed earlier, for small but nonzero ϵ, the outer region of the membrane will have a catenoid shape, and there will be an elastic boundary layer near the small ring. This elastic boundary layer allows the attainment of the point force limit, $r_0 \to 0$, in contrast to the case of the soap film. We begin with the analysis of the case of small axial separation, $h_0 \ll 1$.

A Small displacements

When $h_0 \ll 1$, it is most convenient to work in the Monge parametrization, in which the surface is represented by its height $z(r)$ above the plane $z = 0$. To leading order in h_0, $s \approx r$, and the Euler-Lagrange equation reduces to

$$\epsilon\nabla^4 z - \nabla^2 z = 0, \tag{17}$$

with

$$\nabla^2 = \frac{1}{r}\frac{\mathrm{d}}{\mathrm{d}r}\left[r\frac{\mathrm{d}}{\mathrm{d}r}\right]. \tag{18}$$

The boundary conditions at the large ring $r = 1$ are $z = 0$ and the condition of zero moment, $\nabla^2 z = 0$. At the inner ring $r = r_0$, the displacement $z = h_0$ and the slope $\mathrm{d}h/\mathrm{d}r = 0$.

At order ϵ^0, the outer solution satisfies $\nabla^2 z_{\mathrm{outer}}(r) = 0$, *i.e.*

$$z_{\mathrm{outer}}(r) = b_1 + b_2 \log r. \tag{19}$$

The boundary condition on displacement at $r = 1$ fixes $b_1 = 0$. The zero-moment boundary condition adds no constraint on the solution of (19); b_2 must be determined by matching to the inner solution.

Note that the outer solution diverges at the inner ring as $r_0 \to 0$; the inner solution must correct for this divergence. To find the inner solution, we expand the region near $r = 0$ with the rescaling $\rho = r/\sqrt{\epsilon}$. Then the inner solution satisfies

$$\frac{1}{\rho}\frac{\mathrm{d}}{\mathrm{d}\rho}\left(\rho\frac{\mathrm{d}}{\mathrm{d}\rho}\right)\left[\frac{1}{\rho}\frac{\mathrm{d}}{\mathrm{d}\rho}\left(\rho\frac{\mathrm{d}}{\mathrm{d}\rho}\right)z_{\mathrm{inner}} + z_{\mathrm{inner}}\right] = 0, \tag{20}$$

or

$$\frac{z_{\mathrm{inner}}(\rho)}{h_0} = c_1 + c_2\log\rho + c_3 I_0(\rho) + c_4 K_0(\rho), \tag{21}$$

where $I_0(\rho)$ and $K_0(\rho)$ are modified Bessel functions. c_3 must vanish, since $I_0(\rho)$ diverges as $\rho \to \infty$ and cannot be matched to the outer solution. The boundary conditions at $r = r_0$, or $\rho = r_0/\sqrt{\epsilon}$, add two more constraints to yield

$$\frac{z_{\mathrm{inner}}(\rho)}{h_0} = 1 + c_4\left[K_0(\rho) - K_0\left(\frac{r_0}{\sqrt{\epsilon}}\right) + \frac{r_0}{\sqrt{\epsilon}}K_1\left(\frac{r_0}{\sqrt{\epsilon}}\right)\log\left(\frac{\rho\sqrt{\epsilon}}{r_0}\right)\right]. \tag{22}$$

To match the inner and outer solutions, note that $K_0(\rho)$ decays exponentially at large ρ. Therefore, the constant terms of z_{inner} must vanish, and the coefficient of the logarithmic term of z_{inner} must match b_2. To leading order, we find

$$\frac{z_{\mathrm{outer}}}{h_0} = \frac{\frac{r_0}{\sqrt{\epsilon}}K_1(\frac{r_0}{\sqrt{\epsilon}})\log r}{\frac{r_0}{\sqrt{\epsilon}}K_1(\frac{r_0}{\sqrt{\epsilon}})\log r_0 + K_0(\frac{r_0}{\sqrt{\epsilon}})}, \tag{23}$$

and

$$\frac{z_{\mathrm{inner}}}{h_0} = \frac{\frac{r_0}{\sqrt{\epsilon}}K_1(\frac{r_0}{\sqrt{\epsilon}})\log r + K_0(\frac{r}{\sqrt{\epsilon}})}{\frac{r_0}{\sqrt{\epsilon}}K_1(\frac{r_0}{\sqrt{\epsilon}})\log r_0 + K_0(\frac{r_0}{\sqrt{\epsilon}})}. \tag{24}$$

The Bessel function $K_0(r/\sqrt{\epsilon})$ cancels the logarithmic divergence of the $\log r$ term of the inner solution. To construct a uniformly valid approximation $z_{\rm composite}(r)$ for both the inner and outer regions, we add the two solutions and subtract their common part; this procedure yields the very compact result

$$z_{\rm composite} = z_{\rm inner}\ . \tag{25}$$

It is now clear why a small amount of bending elasticity allows a membrane to support a point force; the elastic boundary cuts off the divergence of the logarithm of the outer solution. To find the solutions in the limit of a point force, recall $K_1(r_0/\sqrt{\epsilon}) = \sqrt{\epsilon}/r_0 + \mathcal{O}(r_0/\sqrt{\epsilon})$ and $K_0(r_0/\sqrt{\epsilon}) = -\gamma + \log(2\sqrt{\epsilon}/r_0) + \mathcal{O}((r_0/\sqrt{\epsilon})^2)$, where $\gamma \approx 0.577...$ is the Euler constant. Thus

$$z_{\rm composite}(r) = h_0 \frac{\log r + K_0(r/\sqrt{\epsilon})}{-\gamma + \log(2\sqrt{\epsilon})}. \tag{26}$$

Note that the boundary condition $z_{\rm composite}(1) = 0$ is satisfied up to terms of order $\epsilon^{1/4}\exp(-1/\sqrt{\epsilon})/\log\epsilon$ for small ϵ.

When $r_0 \to 0$, the elastic boundary layer becomes a small disc of approximate radius $\sqrt{\epsilon}$ around the point force. Thus, the outer solution is roughly the catenoid that connects a ring of radius unity with a ring of radius $\sqrt{\epsilon}$. As we saw in the previous section, the maximum ring separation for a soap film in this situation is approximately equal to the radius of the smaller ring. Thus, as h_0 increases, the amplitude of the catenoid increases until h_0 is of order $\sqrt{\epsilon}$. Since the amplitude of the catenoid cannot increase beyond this value, the boundary layer deforms into a thin cylinder to accommodate further increases in h_0. The formation of the tether is a smooth process; there is no bifurcation.

B Tether: analytical approach

1 *Tether radius, tether stability, and axial force*

Tether formation is an intrinsically nonlinear phenomenon, and to give a complete account of the tether shape we must resort to numerical methods. However, many features of the tether are amenable to an analytic approach. The most prominent such feature is the tether radius. Our numerical calculations will verify that the tether has a cylindrical shape away from the end cap and the catenoid junction to the ring. Thus, for our soap film geometry with $\Delta p = 0$, the radius follows from (5) with constant mean curvature and vanishing Gaussian curvature:

$$2\epsilon H^3 - H = 0. \tag{27}$$

Since $H = -1/(2a)$ for a cylinder of radius a, the exact tether radius $a = \sqrt{\epsilon/2}$ [1]. This square-root dependence of tether radius on inverse tension has been verified experimentally by Evans and Yeung [1].

To study the stability of a cylindrical tether, we write $r(z) = a + u(z)$ and expand the elastic energy (4) to $\mathcal{O}(u^2)$ (to express the metric (7) and mean curvature (8) as functions of z we use $\mathrm{d}z/\mathrm{d}s = \sqrt{1 + r'(z)^2}$), yielding

$$\frac{\mathcal{E}}{2\pi} = \int \mathrm{d}z \left[\left(a + \frac{\epsilon}{2a}\right) + \left(1 - \frac{\epsilon}{2a^2}\right)\left(u + \frac{au'^2}{2}\right) + \frac{\epsilon a}{2}\left(u''^2 + \frac{u^2}{a^4}\right)\right]. \tag{28}$$

A total derivative term has been dropped in (28). We recover the equilibrium tether radius by minimizing the u-independent terms over a. The terms linear in u vanish as expected when a takes the equilibrium value $\sqrt{\epsilon/2}$. Note that the terms quadratic in u' vanish in equilibrium as well since the terms u and $au'^2/2$ always enter in the combination $u + au'^2/2$ arising from the combination $r\sqrt{1 + r'^2}$ in the original energy. Since the remaining terms of Eq. (28) in u^2 and u''^2 are positive definite, the tether is stable. Therefore, the *equilibrium* cylinder solution does not undergo a pearling instability [37, 38]. These considerations suggest that the pearling behavior induced by a rapid pull of a membrane tether [39] arises because hydrodynamic resistance prevents the radius from instantly assuming the value appropriate to the new value of tension. This mechanism differs in detail from that of the laser-tweezer-induced instability of membrane tubes with fixed volume [38].

The tether radius determines the axial force. For an undistorted cylinder with $u = 0$ and equilibrium radius $a = \sqrt{\epsilon/2}$, the total energy per unit length $\mathcal{E}/L = 2\pi\sqrt{2\epsilon}$. Therefore, the axial force $F/(2\pi) = \sqrt{2\epsilon}$ saturates to a constant value independent of tether length once the tether has formed. Since the axial force is independent of z, the junction connecting the tether to the ring is a catenoid with $b = \sqrt{2\epsilon}$. Note that the minimum attainable radius of the limiting catenoid is twice the radius of the tether. Thus, the catenoid cannot smoothly join onto the cylindrical tether; there must be a transition region. Before analyzing this transition region in more detail, we consider the role of pressure.

2 *The effects of pressure are subleading*

Evans and Yeung argued that the pressure jump Δp, present in the case of a closed vesicle under tension, plays little direct role in determining the tether radius [1]. Since a sphere of radius R_0 has constant mean curvature $1/R_0$ and Gaussian curvature $1/R_0^2$, the Euler-Lagrange equation (5) in the spherical region of the vesicle reduces to the Young-Laplace law, $2H = \Delta p$ (even in the presence of bending resistance). If we measure lengths in units of R_0 (for this paragraph only), then the Euler-Lagrange

equation in the region of the tether becomes

$$\frac{\epsilon}{2a^3} - \frac{1}{a} + 2 = 0, \tag{29}$$

since the pressure jump is everywhere uniform. For small ϵ, the three solutions are

$$a = \pm\sqrt{\epsilon/2} + \epsilon/2 + \mathcal{O}(\epsilon^{3/2}) \tag{30}$$

$$a = 1/2 - \epsilon + \mathcal{O}(\epsilon^2). \tag{31}$$

The solution $a = -\sqrt{\epsilon/2} + \mathcal{O}(\epsilon)$ is unphysical. The solution $a = \sqrt{\epsilon/2} + \mathcal{O}(\epsilon)$ corresponds to the tether in the case $\Delta p = 0$. Thus, to leading order, the tether radius is unchanged and the effect of pressure appears at order ϵ. Finally, the solution with a radius near $1/2$ corresponds to a balance of pressure and tension, and is not relevant for tethers.

Returning to our model problem with $\Delta p = 0$, an apparent paradox arises. Since an axial force is required to pull the tether out of the membrane disc, there must be a tension in the membrane. This tension is isotropic, since the membrane is fluid. But consider the cylindrical portion of the tether between two fixed values of z. If this cylinder is cut in half along the long axis (Fig. 5), then each half apparently experiences a force due to the tension. What force balances this tension force if $\Delta p = 0$?

The paradox is most readily resolved by comparing the Euler-Lagrange equations of the variational approach with the equations which follow from force and moment balance on a membrane element, given the lipid bilayer membrane constitutive relation [1]. In the appendix we recapitulate the comparison between the two approaches to the equilibrium shape equations. There it is shown that the coefficient μ of the area term in the variational energy is the tension only for minimal surfaces: $\mu = \Sigma + \epsilon H^2$, where Σ is the tension. Since the pressure jump $\Delta p = 0$, the cylindrical region of the membrane is in a state of pure bending: $\Sigma = 0$. But due to the differential stretching inherent in bending, the outer sheet is stretched and the inner sheet is compressed (Fig. 5). Since the sheets are fluid, the tension or compression in each sheet is isotropic. The compressive and tensile forces along the lines of longitude of the cylinder cancel (consistent with $\Delta p = 0$). However, since the outer sheet is longer than the inner sheet along a line of latitude, there is a net axial tension. The axial force at zero pressure jump is a manifestation of the liquid properties of lipid bilayer membranes.

3 The tether always necks twice

We have seen that the shape of a membrane subject to a point force and under high tension is best described as a boundary layer problem, with tension dominating in the outer region and bending dominating in the inner region. This situation is reminiscent of the coating problems studied by Landau and Levich [15], and Bretherton [16], in which the shapes of different regions of an interface are determined by different balances. The analogy goes further: Bretherton showed that the trailing edge of a large air bubble rising in a capillary tube filled with viscous liquid has a slight ripple [16]. We now show that there are slight ripples in the shape of a lipid membrane at *both* ends of the cylindrical tether region. These ripples have been noticed in the numerical work of ref. [6].

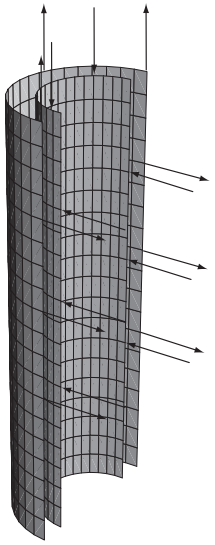

FIG. 5: Axial force due to the greater circumference of the outer leaf.

Since we expect bending and tension to be equally important in the junction region, we must rescale the variables to balance these two effects. Let s_1 be the arclength corresponding to a point in the transition region; we will not specify s_1 any further, except to assume that the radius $r(s_1)$ is small and close to $\sqrt{\epsilon/2}$. It is therefore natural to rescale the radius as in section V., $r = \rho\sqrt{\epsilon}$. The further rescalings $\sigma = (s - s_1)/\sqrt{\epsilon}$ and $\zeta = (z - z(s_1))/\sqrt{\epsilon}$ leads to a balance of the bending and tension terms:

$$\bar{\nabla}^2\bar{H} + 2\bar{H}^3 - 2\bar{H}\bar{K} - \bar{H} = 0, \tag{32}$$

where

$$\bar{H} = \frac{1}{2}\left[\frac{\rho_{\sigma\sigma}}{\zeta_\sigma} - \frac{\zeta_\sigma}{\rho}\right] \tag{33}$$

$$\bar{K} = -\frac{\rho_{\sigma\sigma}}{\rho} \tag{34}$$

$$\bar{\nabla}^2 = \frac{1}{\rho}\frac{\mathrm{d}}{\mathrm{d}\sigma}\rho\frac{\mathrm{d}}{\mathrm{d}\sigma}, \tag{35}$$

$$\tag{36}$$

and $\rho_\sigma^2 + \zeta_\sigma^2 = 1$. Therefore, the transition region is governed by the full nonlinear Euler-Lagrange equation, and there are no further simplifications arising from the smallness of ϵ. However, we can use perturbation theory to study the shape of the transition region near the

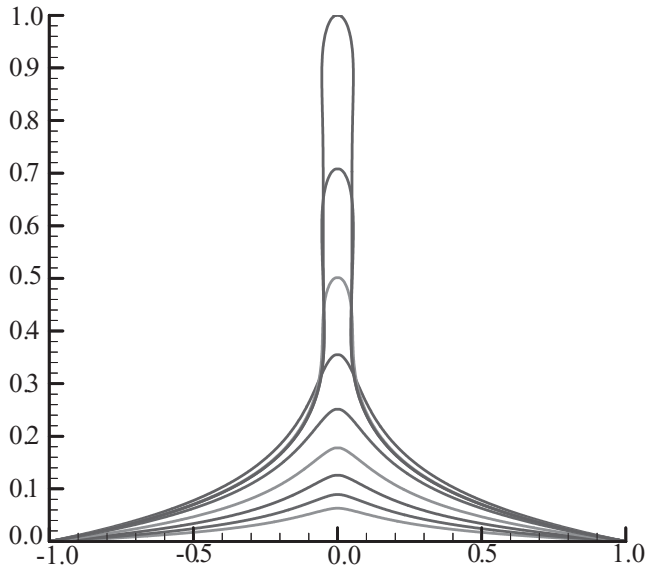

FIG. 6: Membrane shape for various ring separations; $\epsilon = 0.005$ and $r_0 = 0.005$.

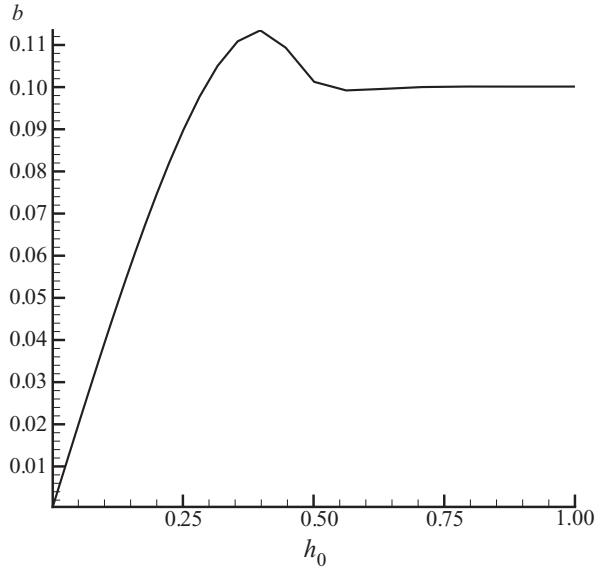

FIG. 7: Force *vs.* displacement; $\epsilon = 0.005$, $r_0 = 0.005$.

tether. Let $\rho = 1/\sqrt{2} + \eta$, with $\eta \ll 1$. To leading order in η, Eq. (32) becomes

$$\eta_{\sigma\sigma\sigma\sigma} + 4\eta = 0. \tag{37}$$

Note that Eq. (37) also follows immediately from Eq. (28) with appropriate rescalings. There are four independent solutions to Eq. (37), each of the form $\eta_\alpha = C_\alpha \exp(ip\sigma)$, where $p = \pm(1 \pm i)$ and $\alpha = 1...4$. The shape near either end of the tether region is an exponentially damped sinusoid with wavelength $2\pi/\sqrt{\epsilon}$ and decay length $\sqrt{\epsilon}$.

C Tether: numerical solution

In the last section we have shown that a description of the membrane shape in the junction region requires the solution of a nonlinear differential equation with no small parameters, despite the smallness of ϵ. Rather than solve this equation numerically and match the solution onto the tether and catenoid regions, we simply solve for the complete shape numerically. We use standard relaxation techniques [40] to solve for the shape as a function of ring displacement h_0, using a small ring of radius $r_0 = 0.001$ to mimic the point force. Figure 6 displays the membrane shape for various h_0. For small h_0, the shape is well-approximated by the linearized catenoid with an elastic boundary layer at small radius (see section V.). As h_0 increases, the amplitude of the catenoid increases until the limiting catenoid with $b = \sqrt{\epsilon}$ is reached. For larger separations, a tether forms. The axial force as a function of displacement is shown in Fig. 7. Note that the force increases to a maximum and then decreases slightly before saturating to $\sqrt{2\epsilon}$. This behavior is reflected in Fig. 6, where the limiting catenoid lies inside the catenoids with slightly lower values of h_0, since these catenoids have slightly larger values of the minimum neck radius $b = F/(2\pi)$. Figure 8 shows the ripple in the junction region. The radial scale has been magnified for clarity.

VI. CONCLUSION

We have seen that tethers in our model problem are a type of boundary layer phenomenon. In the cylindrical tether region, bending dominates, whereas tension dominates at larger radii. The insights we have gained carry over to the more complicated problem of tether formation in closed lipid bilayer membrane vesicles, where the quantitative details of the force *vs.* extension will be different since tension depends on extension. An important extension of the problem considered here would be to study membranes with varying degrees of in-plane order, ranging from liquid-crystalline to solid-like, since the liquid nature of fluid membranes seems crucial for tether formation.

ACKNOWLEDGMENTS

We thank Vikram Deshpande for useful discussions. We acknowledge support from the Brown MRSEC on Micro- and Nanomechanics of Materials (TRP) and NSF Grant DMR9812526 (REG).

*

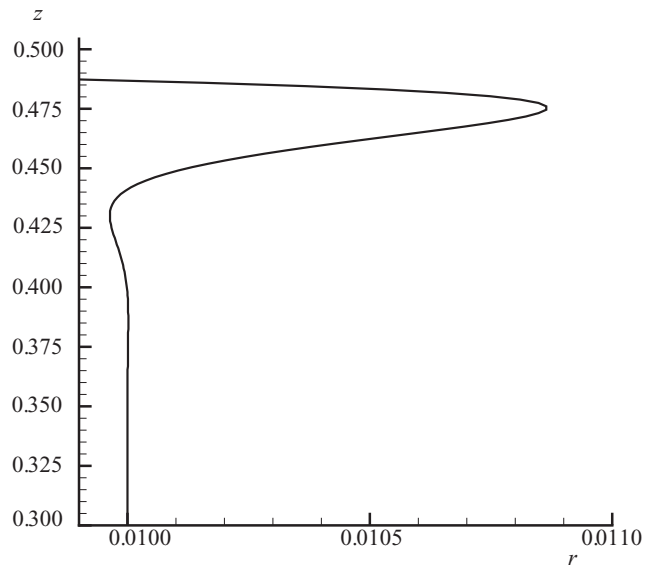

FIG. 8: Ripple, $\epsilon = 0.0002$.

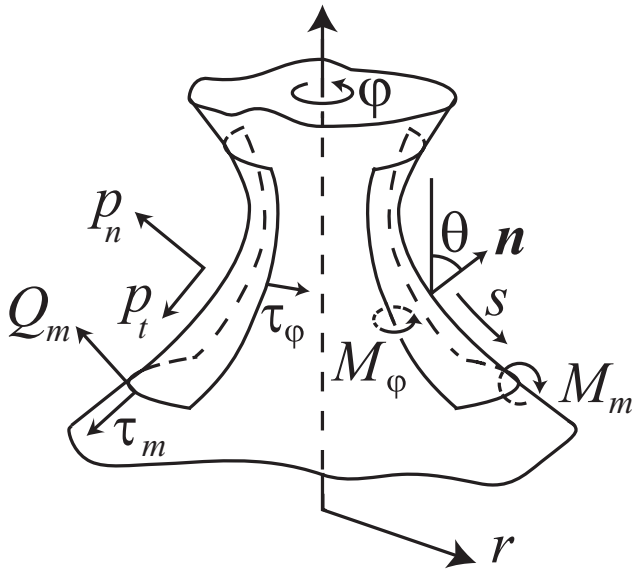

FIG. 9: Forces and moments acting on an element of an axisymmetric membrane.

APPENDIX A: PLATE THEORY VS. VARIATIONAL PRINCIPLE

In this appendix, we recall the force and moment balance relations for axisymmetric shells [1, 41], and review the constitutive relations for fluid membranes [1]. This approach is equivalent to the variational approach taken in the text, and elucidates the apparent paradox discussed in section VB2. Figure 9 shows the forces and moments acting on a small element of fluid membrane. Only the forces and moments that enter the shape equations are shown. τ_m is the force per unit length parallel to the meridian acting on an element edge along the azimuthal direction. τ_φ is the force per unit length in the azimuthal direction acting on an element edge along a meridian. The shearing force Q_m acts along the surface normal on an element edge along the azimuthal direction. The external stresses p_n and p_t are forces per area acting on the element in the normal and meridional directions, respectively. The curvature along the meridian $c_m = \mathrm{d}\theta/\mathrm{d}s$, and the curvature in the azimuthal direction $c_\varphi = \sin\theta/r$.

The balance of forces and moments is just the same as in shells. Normal stress balance requires

$$p_n = \tau_\varphi c_\varphi + \tau_m c_m - \frac{1}{r}\frac{\mathrm{d}}{\mathrm{d}s}(rQ_m). \tag{A1}$$

Tangential stresses balance when

$$-p_t = \frac{1}{r}\frac{\mathrm{d}}{\mathrm{d}s}(r\tau_m) - \frac{\tau_\varphi}{r}\frac{\mathrm{d}r}{\mathrm{d}s} + c_m Q_m, \tag{A2}$$

where we have used $\cos\theta = \mathrm{d}r/\mathrm{d}s$. Moment balance about the φ-axis relates the shearing force Q_m to the moments per unit length M_m and M_φ:

$$Q_m = \frac{1}{r}\frac{\mathrm{d}}{\mathrm{d}s}(rM_m) - \frac{M_\varphi}{r}\frac{\mathrm{d}r}{\mathrm{d}s}. \tag{A3}$$

It is useful to have an expression for the total axial force acting on a circle of latitude. Consider the resultant of the normal and axial stresses along the axial direction:

$$r(p_n\cos\theta - p_t\sin\theta) = \frac{\mathrm{d}}{\mathrm{d}s}\Big(r\tau_m\sin\theta - rQ_m\cos\theta\Big), \tag{A4}$$

where we have used eqns. (A1,A2). In our model problem, the external stresses vanish, $p_n = p_t = 0$. Thus, $r\tau_m\sin\theta - rQ_m\cos\theta$ is a constant, which we identify as the total axial force (up to a factor of 2π) by comparison with the axial force on a soap film, Eq. (12):

$$\frac{F}{2\pi} = r\tau_m\sin\theta - rQ_m\cos\theta. \tag{A5}$$

Returning to the derivation of the shape equations, consider now the tangential forces per unit length τ_m and τ_φ. If x denotes the coordinate across the thickness of the membrane, then

$$\tau_m = \bar{\tau} + c_\varphi M_m, \tag{A6}$$

$$\tau_\varphi = \bar{\tau} + c_m M_\varphi, \tag{A7}$$

where $\bar{\tau}_m = \int \tau_m \mathrm{d}x$, $\bar{\tau}_\varphi = \int \tau_\varphi \mathrm{d}x$, $M_m = \int x\tau_m \mathrm{d}x$, and $M_\varphi = \int x\tau_\varphi \mathrm{d}x$. Part of the "tension" in the membrane comes from the bending moments.

The constitutive relation for the fluid membrane completes the specification of the shape equations. Since the fluid nature implies isotropy, $\bar{\tau}_m = \bar{\tau}_\varphi$. We define the common value of tension as $\tau = \bar{\tau}_m = \bar{\tau}_\varphi$. Likewise,

$$M_m = M_\varphi = \kappa\bar{c} \tag{A8}$$

Thus, the shearing force is known once the curvature of the membrane is known:

$$Q_m = \kappa \frac{\mathrm{d}\bar{c}}{\mathrm{d}s}. \tag{A9}$$

Tangential force balance, Eq. (A2), becomes

$$-p_t = \frac{\mathrm{d}}{\mathrm{d}s}(\bar{\tau} + \frac{1}{2}\kappa\bar{c}^2). \tag{A10}$$

In the absence of flow, the external tangential stresses are zero, and $\tau \equiv \bar{\tau} + \kappa\bar{c}^2/2$ is constant. However, $\bar{\tau}$ and $\bar{c}$ need not separately be constant.

Inserting the constitutive relations into Eq. (A1), the normal stress balance becomes

$$p_n = \tau\bar{c} - \frac{1}{2}\kappa\bar{c}(c_m - c_\varphi)^2 - \kappa\frac{1}{r}\frac{\mathrm{d}}{\mathrm{d}s}\left(r\frac{\mathrm{d}\bar{c}}{\mathrm{d}s}\right). \tag{A11}$$

But since $\bar{c} = 2H$ and $K = c_m c_\varphi$, Eq. (A11) reduces to the Euler-Lagrange equation (5) with $\mu = \tau$.

REFERENCES

[1] E. Evans and A. Yeung, "Hidden dynamics in rapid changes of bilayer shape," Chem. Phys. Lipids **73** (1994) 39.

[2] R.M. Hochmuth, N. Mohandas, and P.L. Blackshear, Jr, "Measurement of the elastic modulus for red cell membrane using a fluid mechanical technique," Biophys. J. **13** (1973) 747.

[3] R.E. Waugh, "Surface viscosity measurements from large bilayer vesicle tether formation. II. Experiments," Biophys. J. **38** (1982) 29.

[4] R.M. Hochmuth, H.C. Wiles, E.A. Evans, and J.T. McCown, "Extensional flow of membrane from cell body to elastic tether II. Experiment." Biophys. J. **39** (1982) 83.

[5] R.M. Hochmuth, J.-Y. Shao, J. Dai, and M.P. Sheetz, "Deformation and flow of membrane into tethers extracted from neuronal growth cones," **70** (1996) 358.

[6] V. Heinrich, B. Božič , S. Svetina, and B. Žekš, "Vesicle deformation by an axial load: from elongated shapes to tethered vesicles," Biophys. J. **76** (1999) 2056.

[7] J. Dai and M.P. Sheetz, "Cell membrane mechanics," in *Laser tweezers in cell biology*, M.P. Sheetz, ed. San Diego: Academic Press 1998 and references therein.

[8] H. Miyamoto and H. Hotani, "Dynamic features of microtubules as visualized by dark-field microscopy," Adv. Biophys. **26** (1990) 135.

[9] M. Elbaum, D.K. Fygenson, and A. Libchaber, "Buckling microtubules in vesicles," Phys. Rev. Lett. **76** (1996) 4078.

[10] D.K. Fygenson, J.F. Marko, and A. Libchaber, "Mechanics of microtubule-based membrane extension," Phys. Rev. Lett. **79** (1997) 4497.

[11] V. Emsellem, O. Cardoso, and P. Tabeling, "Vesicle deformation by microtubules: a phase diagram," Phys. Rev. E **58** (1998) 4807.

[12] N. Sciaky, J. Presley, C. Smith, K.J.M. Zaal, N. Cole, J.E. Moreira, M. Terasaki, E. Siggia, and J. Lippincott-Schwartz, "Golgi tubule traffic and the effects of Brefeldin A visualized in living cells," J. Cell Biology **139** (1997) 1137.

[13] A. Upadhyaya, personal communication.

[14] E. Evans, H. Bowman, A. Leung, D. Needham and D. Tirrell, "Biomembrane templates for nanoscale conduits and networks," Science **273** (1996) 933.

[15] L. Landau and B. Levich, "Dragging of a liquid by a moving plate," Acta Physicochim. URSS **17** (1942) 42.

[16] F.P. Bretherton, "The motion of long bubbles in tubes," J. Fluid Mech. **10** (1961) 166.

[17] L. Landau and E.M. Lifshitz, *Theory of elasticity*, 3rd ed. Oxford: Pergamon Press (1986).

[18] Dirk J. Struik, *Lectures on classical differential geometry,* 2nd ed. New York: Dover Publications, Inc. 1961.

[19] E. Cerda and L. Mahadevan, "Conical surfaces and crescent singularities in crumpled sheets," Phys. Rev. Lett. **80** (1998) 2358.

[20] S. Cohn-Vossen, "Unstarre geschlossene Flächen," Math. Annalen **102** (1929) 10.

[21] B. Audoly, "Rigidifying curves on surfaces," C.R. Acad. Sci. I-Math. **328** (1999) 313.

[22] E. Chater and J.W. Hutchinson, "Mechanical analogs of coexistence phases," in *Phase transformations and material instabilities in solids*, M.E. Gurtin, ed. Orlando: Academic Press, 1984.

[23] R. da Silveira, S. Chaieb, and L. Mahadevan, "Rippling instability of a collapsing bubble," Science **287** (2000) 1468.

[24] Y.J. Chen and P.H. Steen, "Dynamics of inviscid capillary breakup: collapse and pinchoff of a film bridge," J. Fluid Mech. **341** (1997) 245.

[25] U. Seifert, "Configurations of fluid membranes and vesicles," Advances in physics, **46** (1997) 13.

[26] B. Alberts, D. Bray, J. Lewis, M. Raff, K. Roberts, and J.D. Watson, *Molecular biology of the cell, 3d ed.* New York: Garland Publishing, Inc., 1994.

[27] P. Canham, "The minimum energy of bending as a possible explanation of the biconcave shape of the human red blood cell," J. Theor. Biol. **26** (1970) 61.

[28] W. Helfrich, "Elastic properties of lipid bilayers: theory and possible experiments," Z. Naturforsch. **29c** (1973) 693.

[29] W. Helfrich, "Blocked lipid exchange in bilayers and its possible influence on the shape of vesicles," Z. Naturforsch. **29c** (1974) 510.

[30] E.A. Evans, "Bending resistance and chemically induced moments in membrane bilayers," Biophys. J. **30** (1974) 923.

[31] E.A. Evans, "Minimum energy analysis of membrane deformation applied to pipet aspiration and surface

adhesion of red blood cells," Biophys. J. **30** (1980) 265.

[32] B. Božič , S. Svetina, B. Žekš, and Waugh, "The role of lamellar membrane structure in tether formation from bilayer vesicles," Biophys. J. **61** (1992) 963.

[33] L. Miao, U. Seifert, M. Wortis, and H.-G. Döbereiner, "Budding transitions of fluid-bilayer vesicles: the effect of area difference elasticity," Phys. Rev. E **49** (1994) 5389.

[34] E. Evans and W. Rawicz, "Entropy-driven tension and bending elasticity in condensed-fluid membranes," Phys. Rev. Lett. **64** (1990) 2094.

[35] W. Rawicz *et al.*, "Effect of chain length and unsaturation on elasticity of lipid bilayers," Biophys. J. **79** (2000) 328.

[36] Ou-Yang Zhong-can and W. Helfrich, "Bending energy of vesicle membranes: general expressions for the 1st, 2nd, and 3rd variation of the shape energy and applications to spheres and cylinders," Phys. Rev. **A39** (1989) 5280.

[37] R. Bar-Ziv and E. Moses, "Instability and 'pearling' states produced in tubular membranes by competition of curvature and tension," Phys. Rev. Lett. **73** (1994) 1392.

[38] R.E. Goldstein, P. Nelson, T. Powers and U. Seifert, "Front propagation in the pearling instability of tubular vesicles," J. Phys. II (France) **6** (1996) 767.

[39] R. Bar-Ziv, E. Moses and P. Nelson, "Dynamic excitations in membranes induced by optical tweezers," Biophys. J. **75** (1998) 294.

[40] W.H. Press, S.A. Teukolsky, W.T. Vetterling, and B.P. Flannery, *Numerical recipes in C*, 2nd ed. Cambridge: Cambridge University Press, 1992.

[41] A.E.H. Love, *A Treatise on the Mathematical Theory of Elasticity*, 4th ed. (Dover Publications, New York, 1944).